Desalination and Water Treatment
www.deswater.com
doi: 10.5004/dwt.2021.27944

244 (2021) 157–166
December

Investigation on hydrocyclone for increasing the performance by modification of geometrical parameters through CFD approach

S. Venkatesh[a,*], S.P. Sivapirakasam[a], M. Sakthivel[b], R. Krishnaraj[c], T.J. Leta[c]

[a]*Department of Mechanical Engineering, National Institute of Technology, Tiruchirappalli, India, emails: venkatesme2014@gmail.com (S. Venkatesh), spshivam@nitt.edu (S.P. Sivapirakasam)*
[b]*Mechanical Engineering, Regional Centre Anna University, Coimbatore, India, email: sakthi_vel_m@yahoo.com*
[c]*Centre for Excellence in Technology Transfer and Incubation, Dambi Dollo University, Ethiopia, emails: prof.dr.krishnaraj@dadu.edu.et (R. Krishnaraj), laterajule@gmail.com (T.J. Leta)*

Received 27 June 2021; Accepted 27 October 2021

ABSTRACT

In this work, the hydrocyclone geometries namely, overflow diameter, underflow diameter and inlet dimensions are altered for analyzing the performance. The Reynolds Stress Model (RSM) is applied to forecast flow arenas and its radial profiles. The Discrete Phase Model (DPM) is applied to examine the separation effectiveness of particles from water. Three different densities of particles are utilized for analysis. The radial profile curve is validated with the existing LDA experimental results. It is observed that decreasing the inlet dimensions and underflow diameter and increasing the overflow diameter produces good results on pressure drop. The case C hydrocyclone has less pressure drop and good collection efficiency when matched to case B and case A. The case C hydrocyclone produces good performance compared to other two cases (case B and case A) when the particles are in less densities.

Keywords: Hydrocyclone; Flow fields; CFD; Pressure drop; Effect of density; Efficiency

1. Introduction

Hydrocyclones are utilized to separate impurities from liquid [1]. The hydrocyclone separates impurities or particulate matters from liquid or water through centrifugal force. Hydrocyclones are utilized in paper industries, textiles, chemical engineering industries, petroleum industries, mineral processing industries and agricultural industries to remove the impurities from process water or liquid. It is utilized in oil industries to isolate oil from water. It is also utilized in irrigation purposes to separate silt and sand particles from irrigation water. Recently, impact on ecosystem is increased due to combined sewer overflows. It contains many impurities. The hydrocyclones are utilized to remove these contaminants [2]. It is also utilized to remove impurities from storm water [3,4].

The hydrocyclone performance is affected due to its maximum pressure drop. The geometrical parameters also an important factor which affects the separation of particulate matters from water. Therefore, altering the geometrical parameters and studying the flow characteristics of hydrocyclone is required to improve the separation efficiency [5,6]. For geometrical modification and improve the separation performance in coke handling process, the Taguchi method was utilized in previous study [7]. The residence time also plays important role in hydrocyclone performance [8]. Usually, experimental investigations are increase the cost of research work and time. Therefore, many researchers

* Corresponding author.

utilized CFD analysis for the investigation. In CFD analysis RSM and Large eddy simulation models are utilized in previous studies [5,9].

In CFD analysis RSM is applied recently. It is suggested by many researchers due to its suitability to solve complex flow [10]. Li et al. [11] deliberated the effects of inlet velocity and inlet concentrations on the hydrocyclone to improve the performance. The separation characteristics are observed in cylindrical hydrocyclone through different kinds of geometrical parameters [12]. The effects axial wave zone is studied in separation sharpness by CFD analysis. In that analysis, particle separation efficiency has been analyzed by DPM for different size of the particles. In addition, flow pattern has been obtained for the various size of the particles [13]. The separation effectiveness is affected due to misplacement of particles. The separation sharpness has been improved by altering the spigot geometry in previous study [14]. Hydrocyclone flow characteristics were examined by Laser Doppler Anemometry (LDA) by Quteishat [15]. In that study, axial and tangential velocity radial profiles are created by LDA at different locations. Li et al. [16] examined about the effect of solid rod on flow field in the hydrocyclone. In addition, effect of separation performance has been investigated when solid rod existing in the flow field. The tangential velocity radial profiles has been examined in the exclusion of coke powders from coking waste water [17]. The internal flow pattern has been examined in the oil separation from water by RSM and experimental analysis [18]. Gama et al. [19] studied the removal of impurities from bentonite clay through CFD analysis. Garcia et al. [20] investigated about the performance of mini hydrocyclones through CFD analysis. In that investigation particles are classified through DPM. Padhi et al. [21] studied the effects of various density of particle, sizes and degrees of liberation in the hydrocyclone performance. Moreover, cut-size and grade efficiency curves has been predicted in that research. Hydrocyclones are utilized in mineral processing industries for thickening and classification applications. It is optimized by the differential evaluation algorithm for predicting the best geometries in previous studies [22]. Li et al. [23] investigated the performance of the hydrocyclone by altering the arc shaped vortex finder length through numerical approach. That research concludes that increasing the arc length until 30 mm produces better performance on the collection efficiency. Jing et al. [24] investigated the separation performance of hydrocyclone in the desanding process. In that research, the water is mixed with oil for reducing the viscosity and increasing the desanding effect in oil separation process. Raesi and Maddahian [25] applied air injection methodology in hydrocyclone for enhancing the oil- water separation process. It concludes that the air injection methodology enhances the separation performance.

In past decades, authors predominantly considered circular cross section inlet hydrocyclone for enhance the performance. Moreover, various optimization techniques utilized to alter the geometries of the hydrocyclone like circular inlet, outlet, and height of the cyclone and cone angle for enhance the separation efficiency and reduce the pressure drop. On the other hand, one of the author proposed a rectangular inlet hydrocyclone with new dimensions for industrial applications [15]. In that research, author predicted flow characteristics curves through LDA approach. It is identified that the optimum geometrical parameters are not utilized in the previously proposed rectangular inlet hydrocyclones. Therefore, that proposed rectangular inlet hydrocyclone has high pressure drop. As a result, it produces a lower separation efficiency.

The literature report indicates that the pressure drop in the hydrocyclone is increased because of its geometrical parameters. The separation effectiveness is affected due to this large pressure drop. Due to this reason, most of the impurities are overflow through the outlet tube. As a result of this, contaminant level is increased in the water. It creates a major pollution effects in the water. Moreover, increment in pressure drop affects the energy consumption factor. The purpose of this research work is improving the separation performance by reducing the pressure drop through optimum geometrical parameters and reducing the impurities level in the water.

The literature report indicates that the overflow diameter, underflow diameter and inlet dimensions are openly correlated to the pressure drop and separation sharpness. Thus, in this research, above mentioned dimensions are altered for analysis. The CFD approach is utilized to predict the flow field and separation effectiveness for this altered geometry of the hydrocyclone.

2. Reference model

Quteishat [15] investigated the flow characteristics curves of rectangular inlet Hydrocyclone through LDA approach. In this work, this model is taken as reference model (Case A) for investigating the performance. The literature report indicates that the geometrical parameters namely, inlet height (D_{ih}) and inlet width (D_{ib}), overflow diameter (D_e), and underflow diameter (D_u) have great influence on the performance of hydrocyclone. Therefore, in present simulation, above mentioned four parameters are opted for alteration. Three cases considered in this simulation. Case A is the reference model. In case B and case C, above mentioned four geometrical sizes are altered and remaining parameters considered same as case A. The inlet height is decreased from 76.2 to 66.2 mm. The inlet width is decreased from 63.5 to 53.5 mm. The underflow diameter is decreased from 38.1 to 30.1 mm. The overflow diameter is increased from 76.2 to 86.2 mm (From case A to case B).

As per the literature report, increment in the inlet height and width increases the head. As a result, it increases the pressure drop because the pressure drop is directly proportional to head. Therefore, in this work, the inlet height and width dimensions are decreased until 63.5 mm and 53.5 mm respectively. Further decrement in the inlet dimensions beyond this limit decreases the particle loading capability. It directly affects the collection efficiency. Moreover, it reduces the pressure drop drastically. Drastic reduction in pressure drop beyond a certain limit leads to poor collection efficiency when the high dense particles are existing in the fluid. It may create a fouling or particles are settled at the inlet. Moreover, overflow diameter is indirectly proportional to the head. Therefore, increasing the overflow diameter decreases the head. As a result, it decreases the pressure drop. In this work, maximum increment of the

overflow diameter is 86.2 mm. It is noted that increasing the overflow diameter beyond this limit produces drastic decrement in pressure drop. It affects the efficiency when the high dense particles are flow with water. The geometrical size details of these three cases are given in Table 1. The layout drawing of the hydrocyclone is shown in Fig. 1.

3. CFD analysis

3.1. Numerical settings and schemes

The RSM utilizes seven additional transport equations for solving the 3D complex flows. Moreover, it applies the RANS equations for solving the Reynolds stresses through the transport equations [26]. In addition, it utilizes dissipation rate for solving this equations. Furthermore, RSM is a best suitable model for solving the flows like swirl, rapid changes in strain rate, streamline curvature and rotational flows in rigorous way compare to other turbulence models [26]. RSM is suitable for solving complex flow problems because greater grid refinement is possible near the wall in this scheme. Hence, RSM is opted in present simulation instead of k-ε model. The Ansys Fluent 15.0 simulation package is employed in this simulation [5].

3.2. Equations for turbulence model

The continuity equations for incompressible flow flow in hydrocyclone can be written as [26]

$$\frac{\partial \overline{u_i}}{\partial x_i} = 0 \tag{1}$$

where x_i is the position, $\overline{u_i}$ is the mean velocity.

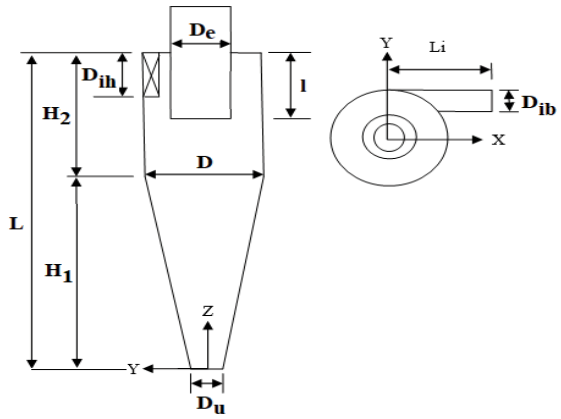

Fig. 1. Layout drawing of Hydrocyclone.

The momentum equation can be written as:

$$\frac{\partial \overline{u_i}}{\partial t} + \overline{u_j}\frac{\partial \overline{u_i}}{\partial x_j} = -\frac{1}{\rho}\frac{\partial \overline{P}}{\partial x_i} + \upsilon\frac{\partial^2 \overline{u_i}}{\partial x_j \partial x_j} - \frac{\partial}{\partial x_j}R_{ij} \tag{2}$$

where ρ is the liquid density, υ is the kinematic viscosity of liquid, $\overline{P}$ is the mean pressure.

$$R_{ij} = \overline{u_i' u_j'} \tag{3}$$

R_{ij} is the Reynolds stress tensor.
where u_i' is the fluctuating velocity component, it can be written as:

$$u_i' = u_i - \overline{u_i} \tag{4}$$

Finally the RSM equation can be written as:

$$\frac{\partial}{\partial t}R_{ij} + \overline{u}_k\frac{\partial}{\partial x_k}R_{ij} = \frac{\partial}{\partial x_k}\left(\frac{v_t}{\sigma^k}\frac{\partial}{\partial x_k}R_{ij}\right) - \left[R_{ik}\frac{\partial \overline{u_j}}{\partial x_k} + R_{ik}\frac{\partial \overline{u_i}}{\partial x_k}\right] - C_1\frac{\varepsilon}{K}\left[R_{ij} - \frac{2}{3}\delta_{ij}K\right] - C_2\left[P_{ij} - \frac{2}{3}\delta_{ij}P\right] - \frac{2}{3}\delta_{ij}\varepsilon \tag{5}$$

The production term equation can be written as:

$$P_{ij} = -\left[R_{ik}\frac{\partial \overline{u_j}}{\partial x_k} + R_{jk}\frac{\partial \overline{u_i}}{\partial x_k}\right],\quad P = \frac{1}{2}P_{ij} \tag{6}$$

where P is the kinetic energy production, v_t is the eddy viscosity.

The transport equation for the turbulence dissipation rate, ε can be written as:

$$\frac{\partial \varepsilon}{\partial t} + \overline{u_j}\frac{\partial \varepsilon}{\partial x_j} = \frac{\partial}{\partial x_j}\left[\left(v + \frac{v_t}{\sigma^\varepsilon}\right)\frac{\partial \varepsilon}{\partial x_j}\right] - C^{\varepsilon 1}\frac{\varepsilon}{K}R_{ij}\frac{\partial \overline{u_i}}{\partial x_j} - C^{\varepsilon 2}\frac{\varepsilon^2}{K} \tag{7}$$

where K is kinetic energy fluctuation, which is given as:

$$K = \frac{1}{2}\overline{u_i' u_i'} \tag{8}$$

The constants are $\sigma^k = 1$, $C_1 = 1.8$, $C_2 = 0.6$, $\sigma^\varepsilon = 1.3$, $C^{\varepsilon 1} = 1.44$ and $C^{\varepsilon 2} = 1.92$.

The DRW scheme is applied to estimate the turbulent dispersion [5].

Table 1
Dimensions of the hydrocyclone

Case	D_{ih} (mm)	D_{ib} (mm)	D_u (mm)	D_e (mm)	D (mm)	L (mm)	H_1 (mm)	H_2 (mm)	l (mm)
Case A	76.2	63.5	38.1	76.2	152.4	562.1	238.25	323.85	189
Case B	71.2	58.5	34.1	81.2	152.4	562.1	238.25	323.85	189
Case C	66.2	53.5	30.1	86.2	152.4	562.1	238.25	323.85	189

The prompt velocity in the *i*th route is quantified as:

$$u_i' = \zeta\sqrt{\overline{u_i'u_l'}} \tag{9}$$

where ζ is the typically dispersed random number. Where u', v' and w' is the reality time of the turbulent eddy. $\sqrt{\overline{u_i'u_l'}}$ is the RMS variation velocity

The life time of the eddy can be written as:

$$T_e = 2T_i \tag{10}$$

Turn over time eddy can be written as:

$$T_e = 0.3K\varepsilon \text{ for the RSTM} \tag{11}$$

$$T_e = -T_i \log r \tag{12}$$

Here, r is the dependable arbitrary number (0 to 1).

The functional magnitude deviates from 0 (far the wall) to 1 (near the wall) [27]. Therefore, this model produces more precise results in contrary pressure gradients. The simulation schemes applied for accurate convergence is provided in Table 2. Furthermore, the accurate convergence is established through the residual value of 10^{-4} [28,29]. The velocity and pressure flow is perceived till they achieve constant. Initially, hybrid initialization is executed for iteration. Afterwards, the iteration is initiated with 0.0001 s. The overall time step is stated as 5 and number iteration per time step is 20.

To obtain the accurate pressure field and to impose mass conversation, the SIMPLE algorithm applies a relations between pressure and velocity correction factors [26]. The QUICK algorithm is utilized when the structured meshes are aligned with direction of flow for improving the calculation accuracy. The second order upwind scheme is utilized for achieving the high order accuracy at cell faces when solving the complex flow problems [26].

3.3. Discrete phase model (DPM)

The particle phase is simulated by the Eulerian-Lagrangian method. One way coupling is employed to resolve the two stage stream. At this point, the water is the nonstop phase and particulates are the sprinkled unconnected phase. The Navier-stokes equation (steady state) is applied in present simulation for solving the water/liquid phase [5,11–14,26]. The Lagrangian frame is applied to analyse the particle trajectory. The crossing point amid the particles are abandoned. The Runge-Kutta frame is employed to solve discrete equations [26].

To enhance the accuracy in particle simulation, assumptions like continuum fluid, 10%–12% fraction volume, perfect elastic condition, feeding of particles small at inlet are considered in DPM [26]. Morsi and Alexander [30] correlations is applied to predict drag coefficient (C_D).

The DPM equations can be written as

$$\frac{du_{\mathrm{Pi}}}{dt} = F_D\left(u_i - u_{\mathrm{Pi}}\right) + \frac{g_x\left(\rho_P - \rho\right)}{\rho_P} \tag{13}$$

Table 2
Solution method

Solution method	Scheme
Pressure-velocity coupling	SIMPLE [5]
Specific dissipation rate	Second order upwind [5,9]
Momentum	Second order upwind [5,9]
Spatial discretization	QUICK
Turbulent kinetic energy	Second order upwind [5,9]

$$\frac{dx_{\mathrm{Pi}}}{dt} = u_{\mathrm{Pi}} \tag{14}$$

$$F_D = \frac{18\mu}{\rho_P d_p^2}\frac{C_D R_e}{24} \tag{15}$$

$$R_e = \frac{\rho d_P \left|u_P - u\right|}{\mu} \tag{16}$$

3.4. Boundary condition

The velocity inlet condition is provided normal to inlet face. The inlet velocity is given as 0.48 m/s. The pressure outlet state is provided at the overflow and underflow ports. The atmospheric pressure is considered at these outlets. The intensity of turbulence is given as 5% (for inlet and outlet). The given hydraulic diameter value at the inlet is 0.0692 m. Density of water considered in this simulation is 998.2 kg/m^3. Viscosity considered for the simulation is 0.001003 kg/ms. Remaining surfaces of the hydrocyclone are considered as walls (No slip condition is given). For the particle simulation, the escape condition is opted at the overflow port. Trap condition is given at the underflow port. Reflect condition is given at the remaining walls. The mass flow rate of the particulate is 20 g/s. Uniform particle size is considered for simulation. In this simulation, particle sizes from 5 to 170 μm have been utilized for analysis. In each particle size, 7500 number of particles are injected at the inlet port of the hydrocyclone for predicting the collection efficiency. Three different kind of densities utilized for analyzing the efficiency. The particle densities considered for analysis are 2,800; 3,800 and 4,800 kg/m^3.

3.5. Mesh generation and validation

The solid model is developed in PTC-CREO package. Finite Volume Method (FEM) is applied to develop hexahedral grids which is shown in Fig. 2. High smoothing and fine relevance center choice is opted to develop fine grids. In this work, 510890 grids are generated for case A, 509850, grids are generated for case B and 510250 grids are generated for case C. Highest number of grids (Fine) selected for avoiding the computational uncertainty. Grid Independence study (GIS) has been established to validate the grid quality. In GIS, three kinds of grids generated namely, coarse (M1), medium (M2) and fine (M3) grids. The pressure drop is calculated for each kind of grids. The results are

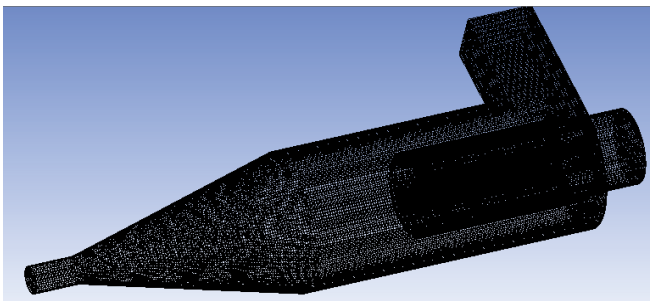

Fig. 2. Hydrocyclone mesh diagram.

provided in Table 3. According to the Richardson's theory, refinement ratio should be greater than 1.3 [31]. Current simulation indicates that the refinement ratio between fine and medium gird is 1.4. Further, refinement ration between medium and coarse grid is 1.42. Moreover, the pressure drop for all kind of grids are almost same. There is no large deviation occurs. These results concludes that the grids are in good quality. Further, it is suitable for simulation.

3.6. Validation of the CFD results

Quteishat [15] generated the axial velocity radial profiles for Hydrocyclone at various axial locations by LDA. In this work, that experimental LDA results are taken for validation. The simulation parameters and geometrical parameters considered in the present simulation is same as that of the Quteishat [15] experiment. Quteishat [15] developed axial velocity radial profile through LDA at Z = 345 mm. In current simulation, the axial velocity profile is created through CFD analysis at the same axial location. The validation profile is given in Fig. 3. It indicates that CFD and LDA results are coincide with each other, tolerable range of discrepancy only occurred between experimental and CFD results. Hence, the present simulation conditions are suitable for investigating the performance of hydrocyclone.

4. Results and discussion

4.1. Pressure field

In this work, the pressure contours of hydrocyclone for the three cases are developed through CFD analysis. These pressure contours are plotted at velocity 0.48 m/s, the contours are shown in Fig. 4. Further, the pressure drop is estimated for the velocities 0.48, 0.58, 0.68 and 0.78 m/s respectively, the plot is shown in Fig. 5. The contour plot indicates that the hydrocyclone pressure drop is increased near the wall region. Further, it is noted that the pressure drop is decreased radially towards the centre axis of the hydrocyclone. At the upper half (cylindrical region) of hydrocyclone, the pressure drop is greater when it is compared to lower half (Conical region). It is noted that the pressure drop slightly increases near the inner tube partition of the vortex finder, it is radially decreases towards the centre axis. The inlet velocity is increased from 0.48 m/s to 0.78 m/s for estimating the pressure drop of the three cases. Lowest pressure drop existing at velocity 0.48 m/s and highest pressure drop existing at velocity 0.78 m/s for these three

Table 3
GIS details

Mesh	No. of elements	Pressure drop (Pa)
M1	256987	312.98
M2	364921	312.36
M3	510890	312.31

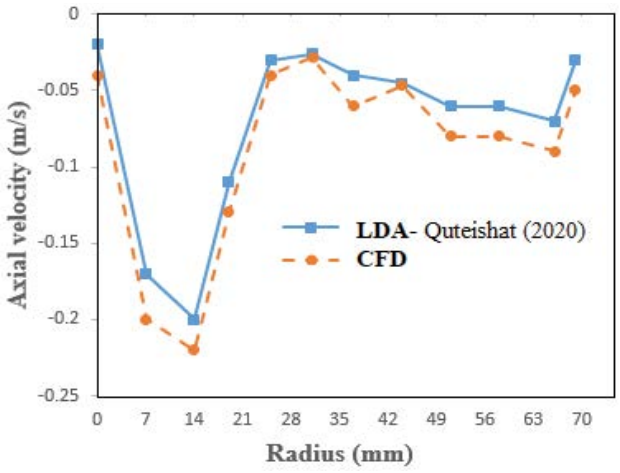

Fig. 3. Validation results at Z = 345 mm (LDA experiment vs. CFD).

cases of the hydrocyclone. The lowest pressure drop for these three cases are 312.3 Pa (Case A), 176.7 Pa (Case B) and 142.1 Pa (Case C) at the velocity of 0.48 m/s. The maximum pressure drop for these three cases are 758.2 Pa (Case A), 337.4 Pa (Case B) and 281.2 Pa (Case C) at 0.78 m/s velocity. The pressure drop in case B is 43.4% less when compared to case A. The pressure drop in case C is 54.5% less when compared to case A. The literature report indicates in past decades, the pressure drop is decreased when decreasing the inlet dimensions of the hydrocyclone. Further, the pressure drop is decreased when increasing the overflow dimensions of the hydrocyclone. In current simulation, the inlet height is decreased from 76.2 to 66.2 mm. The inlet width is decreased from 63.5 to 53.5 mm. The overflow diameter is increased from 76.2 to 86.2 mm. The underflow diameter is decreased from 38.1 to 30.1 mm.

The radial profiles are developed in the axial station of hydrocyclone at Z = 345 mm for these three cases which is shown in Fig. 6. These profiles indicates that the least pressure drop is existing at the case C. the maximum pressure drop is existing at the case A. It shows that the pressure drop reaches its maximum point adjacent the partition region and it is minimum at the middle region. These results conclude that modification of these geometrical parameter size is effectively influences in the pressure drop value. Hence, reduction in pressure drop improve the performance of the hydrocyclone and its collection efficiency.

4.2. Velocity field

The tangential and axial velocities are important factors in the performance of the hydrocyclone. The velocity

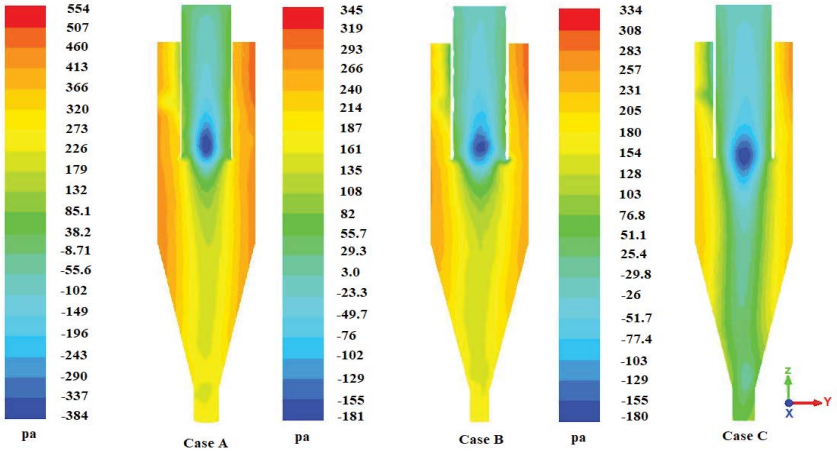

Fig. 4. Pressure contours (Pa) for Case A, Case B and Case C.

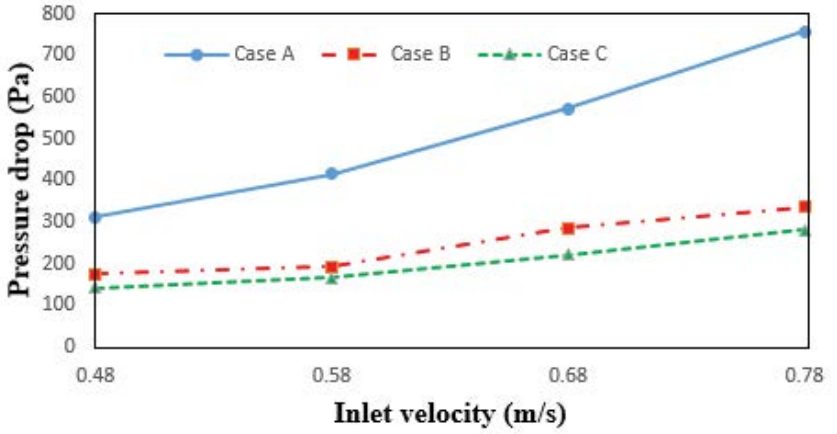

Fig. 5. Pressure drop vs. inlet velocity.

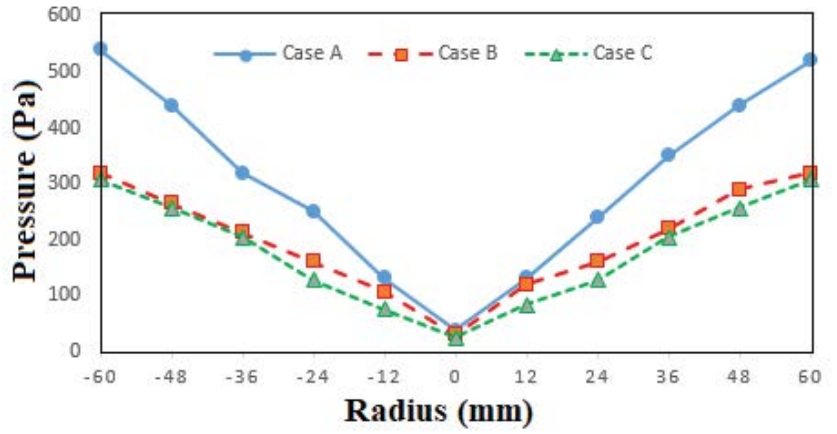

Fig. 6. Pressure drop radial profile.

contours are created for the three different cases of the hydrocyclone at 0.48 m/s velocity. The tangential velocity contours are shown in Fig. 7 and the axial velocity diagrams are shown in Fig. 8. The contour plot indicates that the tangential velocity reaches extreme magnitude at the top portion (near the wall of inlet) of the cylindrical unit. The tangential velocity is maximum at the upper half region of the hydrocyclone and it is tiniest at the lower half region. Further, the tangential velocity is increased at the inner partition of the vortex finder tube and it is gradually

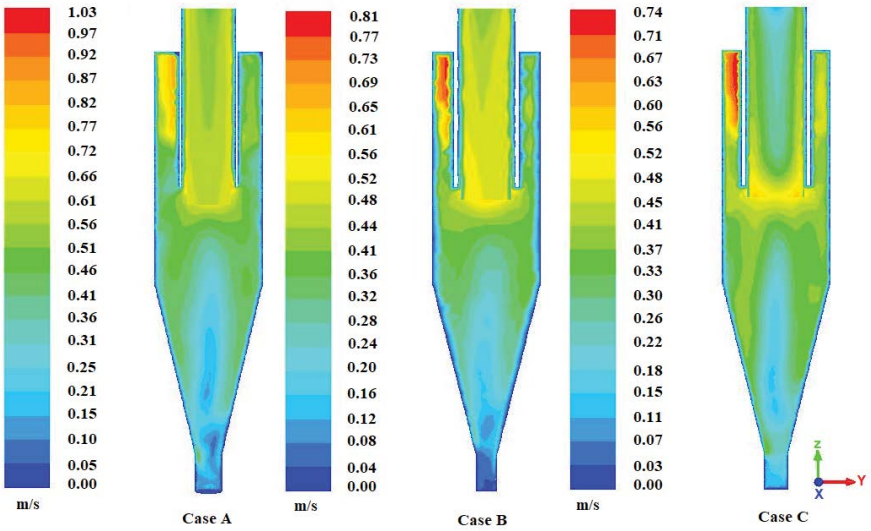

Fig. 7. Tangential velocity (m/s) contours for Case A, Case B and Case C.

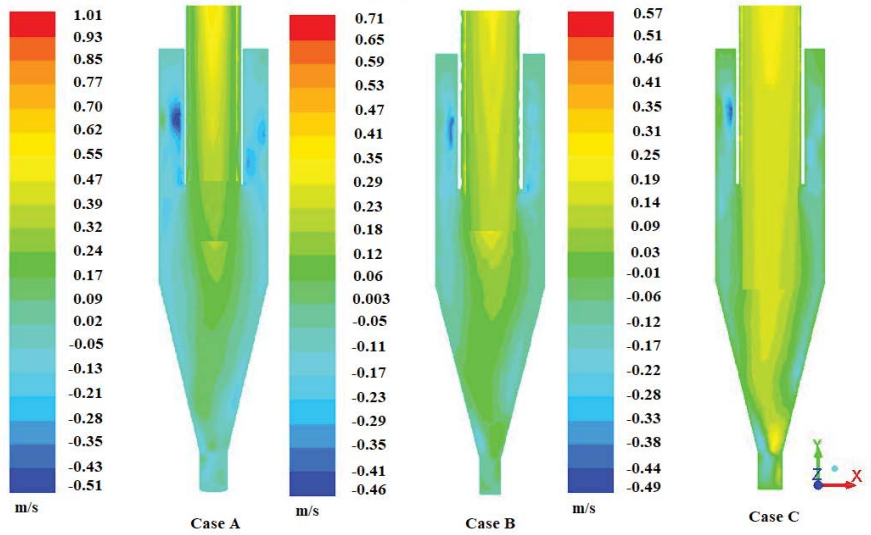

Fig. 8. Axial velocity (m/s) contours for Case A, Case B and Case C.

decreased at the centre point of vortex finder. Similarly, tangential velocity is increased radially until particular point then it is slightly decreased near the wall of the hydrocyclone. It is observed that tiniest tangential velocity is existing at the centre axis of the bottom of the conical section. It indicates that reverse flow is occurred at the inward vortex of the hydrocyclone. Therefore, minimum pressure drop is existing at the bottom half. Hence, the particles are separated from the water and it is settled at bottom through the underflow port. The axial velocity is decreased near the wall region of the hydrocyclone. It is slightly increased at the centre axis. The axial velocity is reached its minimum magnitude at the underflow port and it is reached maximum magnitude in the vortex finder region. In case A and case B, the extreme axial velocity is existing at the inner vortex province when it is linked to case C.

The radial profiles for the tangential and axial velocity are created at the axial location of the hydrocyclone at Z = 345 mm for the three cases. It is shown in Fig. 9. The tangential velocity radial profile shows that the velocity is increases from centre point towards radially until radial point 31 mm. After reaching its maximum point then it is slightly decreased towards the wall. It is looking like M shape curve. The axial velocity profile demonstrates that the velocity is slightly amplified at the centre axis and it is radially decreased until radial point 14 mm. Afterwards, it reaches its peak point at the radial distance of 31 mm from the centre axis. After reaching its peak point then it is little bit diverged from its maximum point until the wall of the hydrocyclone. It is looking like W shape curve. The tangential velocity and axial velocity magnitude is less in the case C when equated to the case B and case

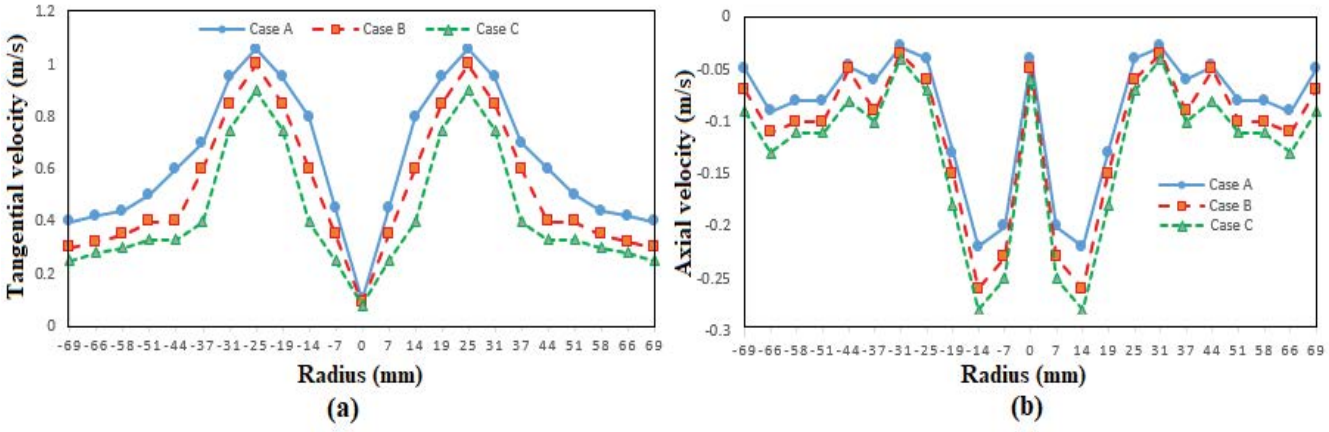

Fig. 9. (a) Radial profile tangential velocity and (b) Radial profile axial velocity for Case A, Case B and Case C.

A. Therefore, the pressure drop of the case C is less when equated to other two cases.

4.3. Efficiency comparison

The DPM has been applied for predicting the efficiency for individual particle size. Three different density of particle is utilized for analyzing the efficiency. The simulation is initiated by 550000 step length factor with 5 number of steps. The particle densities such as 2,800, 3,800 and 4,800 kg/m^3 are utilized in this simulation. The efficiency plots are shown in Fig. 10. The particle efficiency is estimated by taking the ratio of number particles trapped to the number of particles injected. These efficiency plots are indicates that case C produces better collection efficiency compare to case A and case B. The Eq. (17) indicates that the tangential velocity is directly proportional to the pressure drop. Thus, increment in tangential velocity increases the pressure drop. Further, increment in pressure drop in the hydrocyclone decreases the separation efficiency. In present simulation, tangential velocity of the case C hydrocyclone is slightly less when compared to the other two cases (Case A and B). Therefore, it confirms that the case C produces less pressure drop. Moreover, it produces maximum separation efficiency due its less pressure drop.

$$\Delta p = 0.5\ \rho_g V_i^2 H_v \tag{17}$$

Initially, 2,800 kg/m^3 density of particle is injected at the inlet of hydrocyclone. The results show that 50 % of the particles are collected at 80 μm size in case A. Moreover, it is noted that 50% of the particles are gathered at 69 μm size in case B and 50% of the particles are gathered at 58 μm size in case C. It indicates that the case C produces better separation when the particles are in lowest density. The case C hydrocyclone produces maximum efficiency when the particles are in 140 μm. It is 10% higher than the case B and 15% higher than the case A.

Afterwards, 3,800 kg/m^3 density of particle injected for analysis. It is observed that 50% efficiency is obtained at 66 μm for case A. In case B, 50% particles are separated at 54 μm. In case C, 50 % particles are separated at 52 μm. It indicates that separation of particles from water is increased when increasing the density of particles. At 120 μm, the case C produces maximum efficiency. It is noted that collection efficiency of the case C hydrocyclone is 5% higher than the case B and 10% higher than the case A.

Afterwards, 4,800 kg/m^3 density of particle injected for analysis. In case A, 50% efficiency is obtained at 60 μm. In case B, 50% efficiency is obtained at 51 μm. In case C, 50% efficiency is occurred at 40 μm. At 110 μm, the case C hydrocyclone produces maximum efficiency. It is 5% higher than the case B and 8% higher than the case A.

The important objective of this research work is increasing the separation of impurities from water by reducing the pressure drop. The pressure drop and separation performance is directly related to structure and geometrical factors of the rectangular inlet hydrocyclone. Moreover, reducing the pressure drop consumes less energy. Therefore, in this work, the hydrocyclone structure has been tested with different geometries for achieving the better separation efficiency. Four new geometric ratios are proposed from this work for applying the obtained effects in a large scale (remaining factors are the same) which is given in Table 4. These new geometric ratios are useful to enlarge the hydrocyclone for various large scale applications. One can vary all the dimensions of the hydrocyclone by varying the body diameter through this new ratios for different applications.

Table 4
New dimensions of the hydrocyclone

Geometric factors	New ratios
D_{ih}/D	0.435
D_{ib}/D	0.351
D_u/D	0.198
D_e/D	0.566
L/D	3.69
H_1/D	1.57
H_2/D	2.125
L/D	1.24

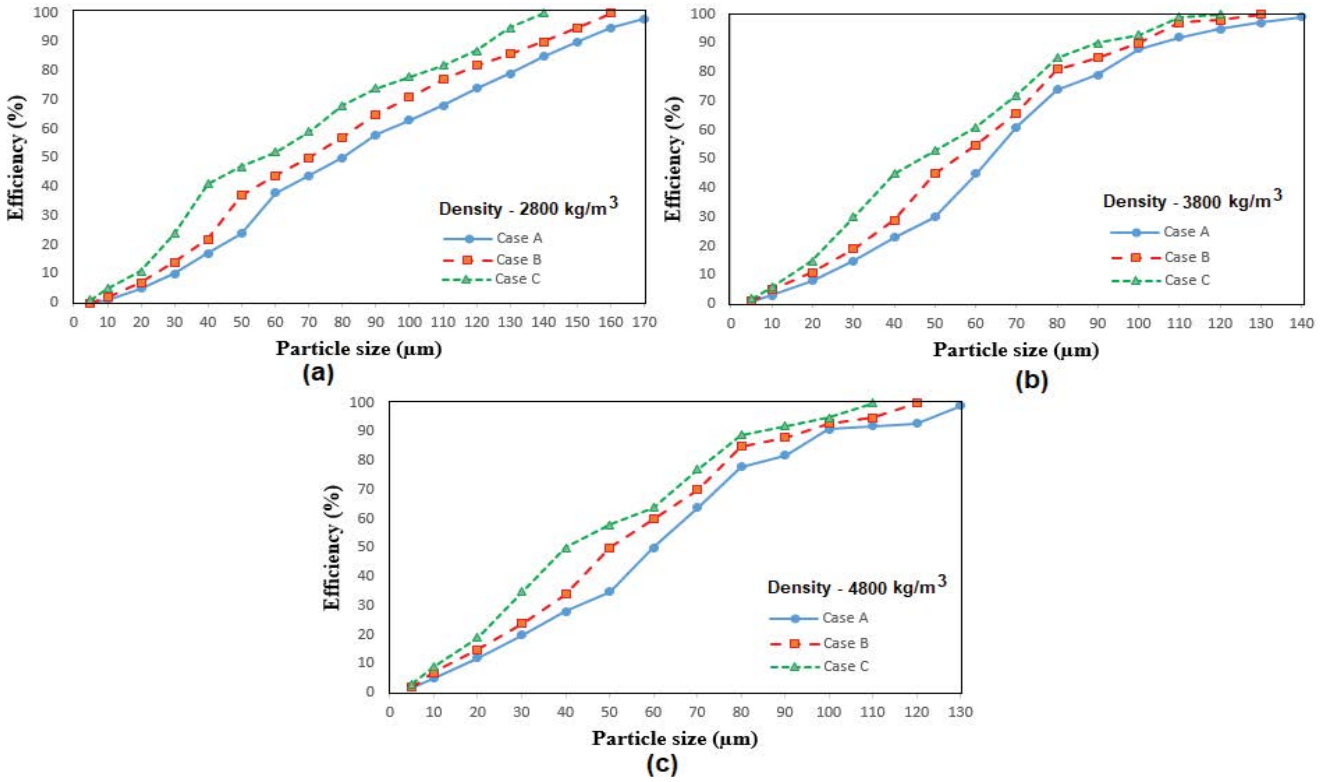

Fig. 10. (a) Efficiency at density 2,800 kg/m^3, (b) efficiency at density 3,800 kg/m^3, and (c) efficiency at density 4,800 kg/m^3.

5. Conclusion

In this work, the rectangular inlet hydrocyclone geometries are modified through CFD analysis. The flow characteristics curves for pressure and velocity is obtained through CFD analysis. The following points are observed in this investigation:

- New geometric ratios are proposed through this investigation. One can apply this new geometric ratios for large scale applications for increasing the separation effects in hydrocyclone.
- Lowest pressure drop existing at velocity 0.48 m/s and highest pressure drop existing at velocity 0.78 m/s for these three cases of the hydrocyclone. The lowest pressure drop for these three cases are 312.3 Pa (Case A), 176.7 Pa (Case B) and 142.1 Pa (Case C) at the velocity of 0.48 m/s. The pressure drop in case B is 43.4% less when compared to case A. The pressure drop in case C is 54.5% less when compared to case A.
- The inlet dimensions namely, decreasing the inlet height 76.2 to 66.2 mm and decreasing the inlet width from 63.5 to 53.5 mm have great influences on minimizing the pressure drop.
- Moreover, increasing the overflow diameter 76.2 to 86.2 mm and decreasing the underflow diameter from 38.1 to 30.1 mm given excellent decrement in pressure drop.
- It is observed that the case C hydrocyclone separate maximum particles from water when compared to other two cases (A and B) and it has less pressure drop compared to other two cases.
- It is observed that case C separates 10% higher particles compared to case B and separates 15% higher particles compared to case A when the density of particle is 2,800 kg/m^3.
- It is noted that collection efficiency of the case C hydrocyclone is 5% higher than the case B and 10% higher than the case A when the density of particle is 3,800 kg/m^3.
- Moreover, separation efficiency of case C is 5% higher than the case B and 8% higher than the case A when the density of particle is 4,800 kg/m^3.

Acknowledgement

This research work is funded by National Institute of Technology, Department of Mechanical Engineering, Tiruchirappalli. The fellowship grant registration ID is 4810006.

Symbols

F_D	—	Drag force, N
ρ_p, ρ_g	—	Particle density, fluid or gas density, kg/m^3
μ	—	Fluid viscosity, kg/ms
μ_t	—	Turbulence viscosity, Pa·s
d_p	—	Particle diameter, m
δ_{ij}	—	Boundary layer thickness
C_D	—	Drag coefficient of particle
u_{pi}	—	Particle velocity, m/s

U	—	Fluid phase velocity, m/s
R_e	—	Relative Reynolds number
x_{pi}	—	Position of particles in i direction
D_{ih}	—	Inlet height, mm
D_{ib}	—	Inlet width, mm
D_e	—	Overflow diameter, mm
D_u	—	Underflow diameter, mm
H_1	—	Length of conical section, mm
H_2	—	Length of cylindrical section, mm
D	—	Hydrocyclone cylinder diameter, mm
L	—	Total length, mm
l	—	Vortex tube length, mm

References

[1] D. Bradley, D.J. Pulling, Flow patterns in the hydraulic cyclone and their interpretation in terms of performance, Trans. Inst. Chem. Eng., 37 (1959) 34–45.

[2] W. Kim, M. Maeng, G. Myung, H. Lee, S. Dockko, Development of a hybrid treatment system for combined sewer overflows using a hydrocyclone and a dissolved air flotation system, Desal. Water Treat., 57 (2016) 7650–7658.

[3] J. Yu, H. Yu, Y. Chen, J. Cheng, Y. Kim, Post treatment schemes of the outflow from hydrocyclone treating paved-road stormwater runoff, Desal. Water Treat., 51 (2013) 4028–4034.

[4] J. Yu, Y. Kim, Hydrocyclone design and energy requirement for treating storm water runoff from bridge, Desal. Water Treat., 57 (2016) 629–635.

[5] Y. Xu, B. Tang, X. Song, Z. Sun, J. Yu, Simulation analysis on the separation characteristics and motion behavior of particles in a hydrocyclone, Korean J. Chem. Eng., 35 (2018) 2355–2364.

[6] R. Sripriya, N. Suresh, S. Chakraborty, B.C. Meikap, Improvement of performance efficiency of a hydrocyclone with design modification by suppressing air core, Korean J. Chem. Eng., 28 (2011) 225–231.

[7] O. Özbakir, S. Koltka, E. Sabah, Modeling and optimization of fine coal beneficiation by hydrocyclone and multi-gravity separation to produce fine lignite clean coal, Part. Sci. Technol., 35 (2017) 712–722.

[8] M.W. Baker, S. Gopalakrishnan, Z. Rogovin, J.D. Miller, Hold-up volume and mean residence time measurements in the air-sparged hydrocyclone, Part. Sci. Technol., 5 (1987) 409–420.

[9] J.A. Delgadillo, R.K. Rajamani, Large-eddy simulation (LES) of large hydrocyclones, Part. Sci. Technol., 25 (2007) 227–245.

[10] Y.L. Chang, W.Q. Ti, H. Wang, S. Zhou, Y. Huang, J.P. Li, G. Wang, Q. Fu, H. Lin, J. Wu, Hydrocyclone used for in-situ sand removal of natural gas-hydrate in the subsea, Fuel, 285 (2021) 1–10.

[11] F. Li, P. Liu, X. Yang, Y. Zhang, Y. Zhao, Effects of inlet concentration on the hydrocyclone separation performance with different inlet velocity, Powder Technol., 375 (2020) 337–351.

[12] F.F. Salvador, G.G. Ascendino, É.V. Faria, M.A. de Souza Barrozo, L.G.M. Vieira, Geometric optimization of filtering cylindrical hydrocyclones, Powder Technol., 381 (2021) 611–619.

[13] Q. Zhao, B. Cui, D. Wei, Y. Feng, Y. He, A.E. Bayly, Linking separation sharpness with the characteristics of axial velocity wave zone in a hydrocyclone, Powder Technol., 386 (2021) 467–482.

[14] D. Hou, B. Cui, Q. Zhao, D. Wei, Z. Song, Y. Feng, Research on the structure of the cylindrical hydrocyclone spigot to mitigate the misplacement of particles, Powder Technol., 387 (2021) 61–71.

[15] M. Quteishat, Hydrocyclone flow characteristics and measurements, Flow Meas. Instrum., 73 (2020) 1–9.

[16] F. Li, P. Liu, X. Yang, Y. Zhang, L. Jiang, H. Wang, Numerical analysis of the effect of solid rod on the flow field and separation performance of thick-walled overflow pipe hydrocyclone, Powder Technol., 388 (2021) 261–273.

[17] S.H. Li, Z.M. Liu, Y.L. Chang, J.P. Li, J.K. Hu, Q.S. Shen, H.L Wang, Removal of coke powders in coking wastewater using a hydrocyclone optimized by n-value, Sci. Total Environ., 752 (2021) 1–10.

[18] S. Li, R. Li, C.G.A. Nicolleau, Z. Wang, Y. Yan, Y. Xu, X. Chen, Study on oil–water two-phase flow characteristics of the hydrocyclone under periodic excitation, Chem. Eng. Res. Des., 159 (2020) 215–224.

[19] A.J.A. Gama, G.A. Neves, P.L. Barros, A.T.P. Neto, J.J.N. Alves, Hydrocyclone performance for bentonite clay purification, Chem. Eng. Res. Des., 161 (2020) 168–177.

[20] D. Vega-Garcia, J.J. Cilliers, P.R. Brito-Parada, CFD modelling of particle classification in mini-hydrocyclones, Sep. Purif. Technol., 251 (2020) 1–9.

[21] M. Padhi, N. Mangadoddy, A.N. Mainza, M. Anand, Study on the particle interaction in a hydrocyclone classifier with multi component feed blend at a high solids content, Powder Technol., 393 (2021) 380–396.

[22] G. Ullmann, S.M. Gonçalves, Y.N. Kyriakidis, M.A. de Souza Barrozo, L.G.M. Vieira, Optimization study of thickener hydrocyclones, Miner. Eng., 170 (2021) 1–12.

[23] F. Li, P. Liu, X. Yang, Y. Zhang, X. Li, L. Jiang, H. Wang, W. Fu, Numerical analysis on the effect of the length of arc-shaped vortex finder on the hydrocyclone's flow field and separation performance, Miner. Eng., 172 (2021) 1–11.

[24] J. Jing, S. Zhang, M. Qin, J. Luo, Y. Shan, Y. Cheng, J. Tan, Numerical simulation study of offshore heavy oil desanding by hydrocyclones, Sep. Purif. Technol., 258 (2021) 1–21.

[25] R. Raesi, R. Maddahian, Numerical investigation of air-injected deoiling hydrocyclones using population balance model, Chem. Eng. Sci., 248 (2022) 1–20.

[26] Fluent, Inc., Fluent 6.1.22 Users' Guide, 2004.

[27] B.E. Launder, N. Shima, Second-moment closure for the near-wall sub layer: development and application, AIAA J., 27 (1989) 1319–1325.

[28] M.M. Gibson, B.E. Launder, Ground effects on pressure fluctuations in the atmospheric boundary layer, J. Fluid Mech., 86 (1978) 491–511.

[29] B.E. Launder, D.B. Spalding, The numerical computation of turbulent flows, Comp. Meth. Appl. Mech. Eng., 3 (1974) 269–289.

[30] S.A. Morsi, A.J. Alexander, An investigation of particle trajectories in two phase flow systems, J. Fluid Mech., 55 (1972) 193–208.

[31] M.D. Slack, R.O. Prasad, A. Bakker, F. Boysan, Advances in cyclone modeling using unstructured grids, Chem. Eng. Res. Des., 78 (2000) 1098–1104.